This full-text paper was peer-reviewed at the direction of IEEE Instrumentation and Measurement Society prior to the acceptance and publication.

Reconstruction of Multi-perforated Burner Flames through Sectioning Tomography and Light Field Imaging

Qi Qi[1], Md. Moinul Hossain[1,] *, *Senior Member*, *IEEE* , Gang Lu[1], *Senior Member*, *IEEE* , Yizhi Huang[2], Chuanlong Xu[2]

[1]School of Engineering, Mathematics and Physics, University of Kent, Canterbury, Kent, CT2 7NT, UK

[2]National Engineering Research Center of Power Generation Control and Safety, School of Energy and Environment, Southeast University, Nanjing 210096, China

q.qi@kent.ac.uk, m.hossain@kent.ac.uk, g.lu@kent.ac.uk, 230189043@seu.edu.cn, chuanlongxu@seu.edu.cn

***Abstract*—Multi-perforated combustors are promising for reducing carbon emissions by improving combustion efficiency and reducing pollutant formation. These systems produce dense flame fields composed of multiple spatially confined and often overlapping flame structures, posing significant challenges for accurate flame image reconstruction, which is essential for combustion analysis and optimization. Existing methods primarily focus on reconstructing multiple depth sections of single flames, which limits their applicability to multi-flame configurations. This study proposes a novel imaging reconstruction approach that integrates sectioning tomography, light field imaging, and digital refocusing to achieve accurate depth-resolved flame images in multi-perforated burners. This method prioritizes accurate reconstruction of individual flame images by reconstructing one representative section per flame. Experiments were carried out on both non-overlapping and overlapping flames to demonstrate the method's ability to reconstruct depth-specific images of complex flame structures. Results show that the proposed method accurately reconstructed flame contours and intensity distributions in non-overlapping flames, while effectively isolating radiative contributions from depth-specific sections in overlapping flames. This strategy captures the overall combustion characteristics while allowing for a detailed analysis of individual flame states, providing a comprehensive understanding of both global and local combustion behaviors. Furthermore, it reduces computational complexity while preserving high-fidelity flame representation, offering an efficient tool for advanced diagnostics in multi-perforated burners.**

Keywords—Multi-perforated burner, Light field imaging, Digital refocus, Reconstruction

I. INTRODUCTION

Reducing carbon emissions (CO_2) is crucial for combating climate change and ensuring a sustainable future. CO_2 significantly contributes to global warming, causing severe environmental impacts [1]. Multi-perforated combustors offer a promising solution for reducing carbon emissions by improving combustion efficiency and lowering pollutant formation. The design of a multi-perforated burner allows for precise air-fuel mixing and staged combustion, which minimises incomplete combustion and reduces CO_2 formation and NOx generation [2]. These advantages make multi-perforated combustors highly suitable for industrial and residential applications, offering an energy-efficient alternative to conventional combustion systems. Accurately measuring the flame images of multi-perforated combustors is essential for optimising combustion efficiency, minimising emissions, and refining combustor design, as it provides critical insights into flame shape, stability, and distribution, which are closely linked to combustion dynamics and pollutant formation [3].

To obtain the flame images of multi-perforated burners, chemiluminescence and imaging-based techniques have been developed. These methods enable non-intrusive and high-resolution visualisation of flame structures by capturing the light emitted from excited chemical species during combustion. These methods allow for detailed analysis of flame characteristics without direct contact. For example, Choi et al. [4] used OH* chemiluminescence and OH planar laser-induced fluorescence (OH-PLIF) techniques to image various hydrogen-enriched flames of a mesoscale burner array. Ge et al. [5] performed experimental studies on the combustion performance of hydrogen-enriched natural gas in a dry low-emission (DLE) burner using the OH-PLIF method. Flame topology, Nox, and CO emissions were analysed. Sun et al. [6] studied the gas concentration and temperature of the multi-nozzle flame through tunable diode laser absorption spectroscopy (TDLAS). However, chemiluminescence-based techniques rely on complex and costly instruments that are not suitable for industrial environments. Imaging-based techniques can capture real-time flame images, allowing the analysis of flame structure, stability, temperature, flame radicals distribution, and so on. Ahmadi et al. [7] utilized a low-noise charge-coupled device (CCD) camera to capture flame images from a cylindrical multi-perforated burner in domestic heating boilers to analyze the thermal performance. Li et al. [8] employed a CCD camera equipped with a specialized 105 mm focal length lens to capture OH* of a micro-jet array burner flame. However, the flame in multi-perforated burners is compact and composed of multiple flames, making it challenging to capture the 3-D information of the flame. Addressing this typically requires either a focus adjustment with a single camera or utilizing multiple cameras to acquire multi-angle imaging. However, such systems are complex and demand a high degree of synchronization and precise control.

To address these challenges of flame imaging in multi-perforated burners, light field (LF) imaging provides a promising solution by capturing both the angular and spatial information of light rays in a single exposure using a single LF camera (LFC) [9]. Based on the Fourier Slice Theorem, Ren et al. [10] introduced a digital refocusing theory that enables image reconstruction at various depths using raw LF data. Zhao et al. [11] applied optical sectioning tomography with LF imaging for 3D flame and temperature measurements, while Liu et al. [12] extended this method to laminar and turbulent diffusion flames. However, previous studies mainly focused on single or turbulent flames. In multi-perforated

burners, where the flames are compact and densely distributed, reconstructing global and local flame characteristics simultaneously is more important than reconstructing multiple sections of a single flame.

This study utilizes the sectioning tomography method, combined with LF imaging and digital refocusing technique, aiming to reconstruct the flame images at different depths in multi-perforated burners. The applicability of the proposed method is evaluated through experimental studies. The refocused depth and point spread function (PSF) of the LF imaging system are obtained through calibrations. The flame images at different depths for various multi-perforated burners are reconstructed. The measurement principles, calibration procedures, and experimental studies are introduced and analyzed in detail.

II. Methodology

Fig. 1 illustrates the overall principle of the proposed method, which comprises three key stages: raw LF image acquisition using a LFC, digital refocusing to generate a depth-resolved image stack, and sectioning tomography based on a deconvolution algorithm incorporating system calibration to reconstruct flame images at selected depths.

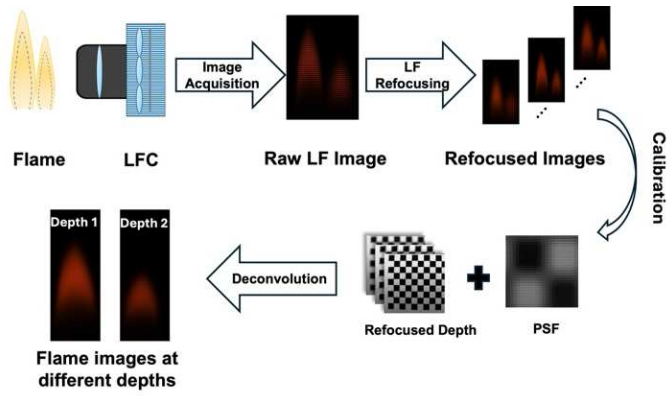

Fig. 1. The principle of the proposed method.

A. Principle of Light Field Imaging and Digital Refocusing

Fig. 2 illustrates the schematic of the LF imaging model. Different from a conventional camera, the LFC incorporates a microlens array (MLA) positioned between the main lens and the photosensor. In the LFC, rays from a single point on the flame converge at a single point on the imaging plane of the main lens. The microlens further separates these rays by their directions, forming sub-images on the pixel array underneath each microlens [13].

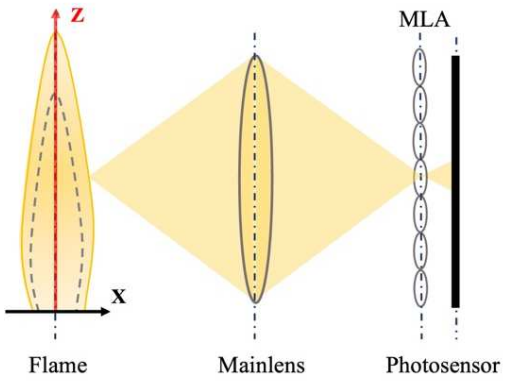

Fig. 2. Schematic of the LF imaging model.

Assuming that both the photosensor plane and lens plane are infinite, and considering the light rays between these two planes, the 4D LF is parameterized as shown in Fig. 3. F is the distance between the lens plane and the photosensor plane, and $\boldsymbol{L_F}(u, v, x, y)$ denotes the radiation distribution of the ray that passes through the lens at (u, v) and strikes the photosensor at (x, y). Therefore, $E_F(x, y)$, the LF image on the photosensor, can be expressed as [11],

$$E_F(x,y) = \iint \boldsymbol{L_F}(u,v,x,y)\,du\,dv \tag{1}$$

The digital refocusing technique can utilize the LF information to calculate the image at depth F', other than F. Assuming that $F'=\alpha F$, where α defines the relative depth. So the $\boldsymbol{L_{\alpha F}}(u, v, x, y)$ can be written as,

$$\boldsymbol{L_{\alpha F}}(u,v,x',y') = \boldsymbol{L_F}\left(u,v,u+\frac{(x'-u)}{\alpha}, v+\frac{(y'-v)}{\alpha}\right) \tag{2}$$

Therefore, $E_{\alpha F}(x', y')$, the LF image on the photosensor corresponding to depth F' is expressed as follows,

$$E_{\alpha F}(x',y') = \iint \boldsymbol{L_F}\left(u,v,u+\frac{(x'-u)}{\alpha}, v+\frac{(y'-v)}{\alpha}\right) du\,dv \tag{3}$$

Based on the above equations, the refocused images under different depths can be calculated by changing the parameter α.

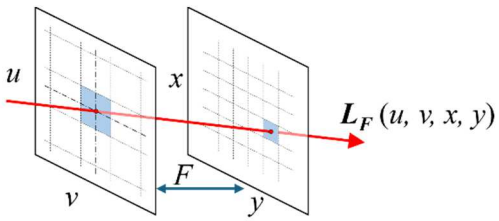

Fig. 3. Parameterization of the 4D LF by two planes.

B. Sectioning Tomography

To isolate and reconstruct flame images at specific depths within the refocused image stack, sectioning tomography is used. According to Fourier Optical Theory [12], the sectioning tomography can be described by a convolution calculation. The response of an imaging system, such as a camera, to a point object is characterized by its PSF. So the flame image intensity $E(x, y, \lambda)$ can be calculated by integrating the convolution along the optical axis direction and is expressed as,

$$E(x,y,\lambda) = \int f(x,y,z,\lambda) * p(x,y,z)\,dz \tag{4}$$

where $*$ denotes the deconvolution operator, $f(x, y, z, \lambda)$ represents the flame radiation intensity distribution at depth z, $p(x, y, z)$ is the PSF of the imaging system at the depth z, and λ is the wavelength. If the overall flame is discretized into N two-dimensional sections, which are parallel to each other and perpendicular to the optical axis of the imaging system, the imaging process can then be represented in a discretized form as,

$$E(x,y,\lambda) = \sum_{i=1}^{N} f_i(x,y,\lambda) * p_i(x,y) \tag{5}$$

The LF imaging system can sharply focus on only one depth (corresponding to one flame section) at a time, while other sections are defocused. These out-of-focus sections still

contribute to the overall image intensity. Due to the translucent nature of flame, separating the in-focus signal from out-of-focus contributions remains a significant challenge [14]. In this study, the Van Cittert algorithm is used to eliminate radiation contributions from defocused planes and reconstruct refocused sections by minimizing the squared error between the recorded image and the estimated image. The corresponding LF-refocused images and the system's PSFs are used to iteratively reconstruct flame images of the refocused sections, progressively removing out-of-focus contributions. Unlike previous work focused on reconstructing multiple sections of a single flame [11, 12], this study focuses on image reconstruction of multiple compact flames in a multi-perforated burner. Due to the compact and small-scale nature of the flames in such burners, reconstructing multiple sections of a single flame becomes less critical. Instead, this work prioritizes the accurate reconstruction of the image of each flame, which is essential for capturing the radiation behavior in multi-flame configurations. Therefore, only one section is reconstructed per flame. This approach not only significantly reduces computational resources and computation time but also effectively reflects the overall combustion state of the flames in the multi-perforated burner.

III. Depth and PSF Calibrations

During the digital refocusing process in LF imaging, each flame section has a relationship between its depth position (d) and an optimal refocusing parameter (s). However, due to the unknown optical structure of the main lens, the mathematical relationship between d and s cannot be directly derived. To address this, a depth calibration was conducted using a black-and-white chessboard placed perpendicular to the optical axis of the LFC. The distance from the chessboard to the front edge of the LFC was precisely measured. A cage-type LFC is used to capture a raw LF image of the chessboard, and a stack of refocused images was generated by varying s. The sharpest image was obtained using the Tenengrad Function, and the corresponding refocusing parameter s was recorded. By repeating this process at various object distances, a relationship between s and d was established. Fig. 4 shows the relationship and the fitted function with a coefficient of determination (R^2) of 0.99719, indicating high accuracy in determining the refocused depth from the refocusing parameter.

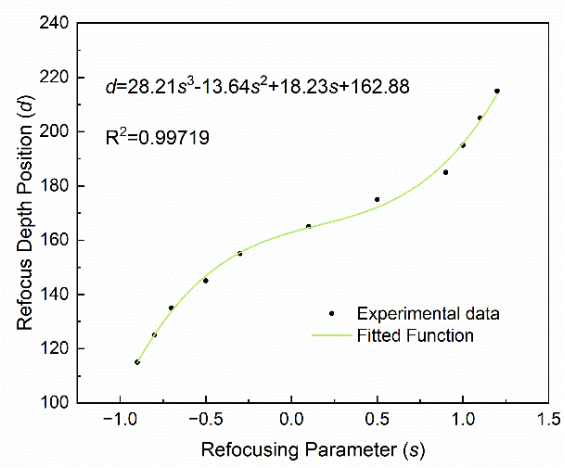

Fig. 4. Refocused depth cabibration result.

After determining the refocused depth for each section of the flame, it is important to calibrate the PSFs for these sections. The PSF calibration method used for conventional cameras can be adapted to refocused images. Among these methods, the Gaussian PSF model is mostly used for optical imaging systems, which is,

$$h(x,y) = \frac{1}{\pi\sigma^2} exp\ (-\frac{x^2+y^2}{2\sigma^2}) \tag{6}$$

where h (x, y) is the Gaussian PSF, and σ is the parameter of the Gaussian PSF determined through calibration. To solve the value of σ, a calibration was carried out based on the edge method [15]. A chessboard with a sharp black-and-white edge is used to capture a straight boundary with the LFC. The intensity variation across the edge in the refocused image is described by the edge spread function (ESF), expressed as,

$$e(x) = \frac{1}{2} erf\left(\frac{x}{\sigma}\right) + \frac{1}{2} \qquad with \tag{7}$$

with

$$erf(x) = \frac{2}{\sqrt{\pi}} \int_{-\infty}^{x} \exp(-t^2)\, dt$$

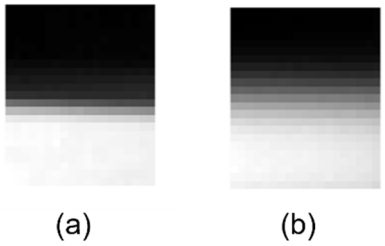

Fig. 5. Refocused images of the straight edge on the chessboard, (a) s=-0.5, (b) s=0.9.

After capturing the straight-edge image, the grayscale values along a line are fitted using Eq. (7) through the least squares method to calculate the parameter σ. Once σ is obtained, the Gaussian PSF can be determined.

In this study, two refocused images corresponding to two flame sections are calculated. Each refocused image represents the accumulation of the radiation distribution from the focused section and the defocused section, resulting in one focused PSF and one defocused PSF for each section. Therefore, a total of 4 PSFs are required for the two flame sections. For example, when the chessboard is placed in the first preset section (s=-0.5), two refocused images (s=-0.5, s=-0.9) of a straight edge between the adjacent black and white grids of the chessboard can be calculated, as shown in Fig. 5. In the same way, the 4 PSF parameters σ of two sections can be determined as follows: $\sigma_{1\text{–}1}$=3.5282 and $\sigma_{2\text{–}1}$=5.2887 represent the σ values of the first and second sections when the system refocuses on the first section, while $\sigma_{1\text{–}2}$=5.3744 and $\sigma_{2\text{–}2}$=3.6522 represent the σ values of the first and second sections when the system refocuses on the second section.

IV. Results and Discussion

To reconstruct the flame images at different depths in multi-perforated burners, the following experimental configuration is employed as shown in Fig. 6. The

experimental setup captures raw LF images of flames using a cage-type LFC. The main lens has a focal length of 50 mm, and the microlens size is 100×100 μm with an f-number of 8. The pixel size of the camera is 5.86 μm. A 600 nm filter is placed in front of the main lens to take advantage of the sensor's higher signal-to-noise ratio at that wavelength. In this paper, multiple candle flames are arranged to substitute for the flames in multi-perforated burners. Fig. 6 (b) illustrates the flame arrangements, which include two distinct configurations: (b1) non-overlapping flames and (b2) overlapping flames. According to the refocused depth calibration result, the front flame corresponds to a refocusing parameter of s=−0.5 (depth=147 mm), and the rear flame to s=0.9 (depth=191 mm).

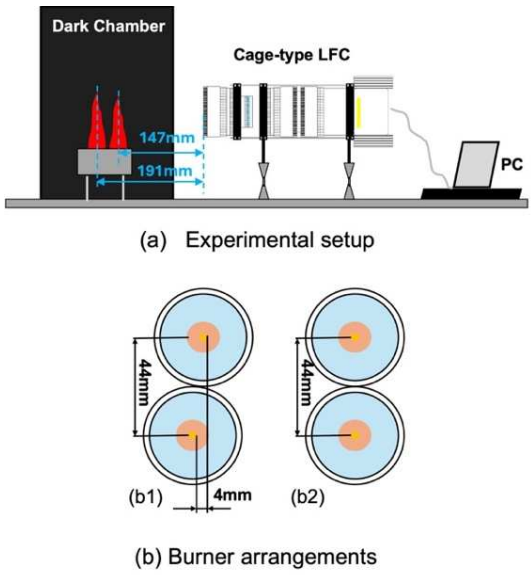

Fig. 6. Schematic of experimental configuration.

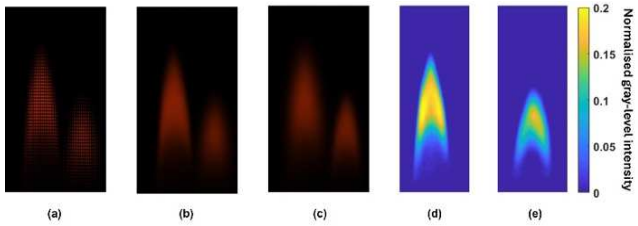

Fig. 7. Reconstructed flame images of non-overlapping flames. (a) Raw LF image, (b) Refocused flame image, s=-0.5, (c) Refocused flame image, s=0.9, (d) Reconstructed flame image, s=-0.5, (e) Reconstructed flame image, s=0.9.

The reconstructed flame images of the non-overlapping flames are shown in Fig. 7. To enhance visual clarity, the images have been subjected to a certain degree of magnification and aspect ratio adjustment. The digital refocusing technique is applied to the raw LF image of non-overlapping flames to obtain refocused images at different depths. It can be seen that when focusing on the front flame, the rear flame appears blurred, and vice versa. This demonstrates that the LF refocusing technique can be used for the reconstruction of flames at different depths. Since the two flames are separate and non-overlapping, the radiation detected by the photosensor corresponds to the radiation of each flame. Fig. 7 (d) and (e) show the reconstructed images of front and rear flames; the images of both the front and rear flames have been reconstructed accurately. Although the rear flame appears relatively small in the image, the overall flame contour and radiation distribution can still be successfully reconstructed.

Fig. 8 shows two representative frames of overlapping flames selected from a continuous image sequence, captured at 0.08 s and 0.15 s, respectively. Compared to the raw LF images captured with non-overlapping flames, the raw LF images obtained with two overlapping flames are brighter and exhibit higher radiation values. This demonstrates that, in the case of overlapping flames, the intensity detected by the photosensor is the cumulative radiative contribution of both flames.

The digital refocusing technique is also applied to the raw LF image of overlapping flames, focusing on the front and rear flames, respectively. The refocusing parameters and refocused depths are consistent with those from the non-overlapping flames. It can be observed that the refocused images at different depths represent the combined contribution of both flames. When focusing on the front flame, the rear flame appears blurred. When refocusing on the rear flame, its boundary becomes visible. However, since the overlap of the two flames, the defocused image of the front flame is still superimposed on the refocused image of the rear flame. The same occurs when focusing on the front flame. Fig. 8 (d) and (e) show reconstructed images of overlapping flames. It can be observed that the reconstructed image of the front flame is similar under both overlapping and non-overlapping conditions. For the rear flame, the reconstructed distribution is less distinct compared to the front flame, as its image appears smaller on the image sensor. Nevertheless, it can still be observed that the intensity is slightly higher along the edges. Although the reconstruction exhibits some missing regions when the flames overlap, especially at the bottom of the front flame, the overall result still successfully captures the flame boundaries and remains acceptable for analysis.

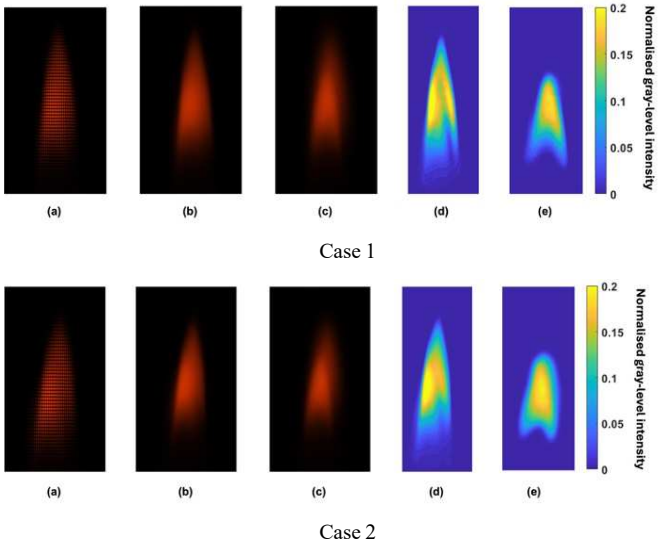

Fig. 8. Reconstructed flame radiation distributions of overlapping flames. (a) Raw LF image, (b) Refocused flame image, s=-0.5, (c) Refocused flame image, s=0.9, (d) Reconstructed flame image, s=-0.5, (e) Reconstructed flame image, s=0.9.

V. Conclusions

This study presents an effective reconstruction method that integrates sectioning tomography, LF imaging, and digital refocusing to achieve accurate depth-resolved flame imaging in multi-perforated burners. Calibrations are conducted to

determine the refocused depth and PSF. The digital refocusing algorithm is used to obtain refocused images at different depths, while the Van Cittert algorithm is utilized to remove the radiation contribution from defocused planes, yielding the original flame image of each reconstructed flame.

To evaluate the performance of the proposed methods, experimental studies are carried out with two flame configurations: non-overlapping flames and overlapping flames. In the non-overlapping case, the method accurately reconstructed the flame contours and intensity distributions at distinct depths. In the overlapping case, the method successfully separated radiation contributions from different layers, demonstrating its ability to handle complex flame structures. Overall, the proposed method shows strong potential for flame diagnostics and can be extended to more realistic combustion systems involving multi-perforated burners and dynamic flame behaviors.

ACKNOWLEDGEMENT

The authors wish to express their gratitude to the Engineering & Physical Sciences Research Council (EPSRC) Project Reference: EP/X020789/1.

REFERENCES

[1] A. Bardos, K. M. Walters, M. G. Boutross, S. Lee, C. F. Edwards, and C. T. Bowman, "Effects of Pressure on Performance of Mesoscale Burner Arrays for Gas-Turbine Applications," Journal of Propulsion & Power, vol. 23, no. 4, pp. 884-886, 2015, doi: 10.2514/1.26255.

[2] S. Lee, M. Svrcek, C. F. Edwards, and C. T. Bowman, "Mesoscale Burner Arrays for Gas-Turbine Reheat Applications," Journal of Propulsion and Power, vol. 22, no. 2, pp. 417-424, 2006, doi: 10.2514/1.15667.

[3] W. J. Liu, B. Ge, Y. S. Tian, Y. W. Yuan, S. S. Zang, and S. L. Weng, "Experimental investigations and large-eddy simulation of low-swirl combustion in a lean premixed multi-nozzle combustor," Experiments in Fluids, vol. 56, no. 2, 2015, doi: 10.1007/s00348-015-1899-5.

[4] J. Choi, W. Lee, R. Rajasegar, T. Lee, and J. Yoo, "Effects of hydrogen enhancement on mesoscale burner array flame stability under acoustic perturbations," International Journal of Hydrogen Energy, vol 46, no 74, pp.37098-37107, 2021, doi: 10.1016/j.ijhydene.2021.08.192.

[5] B. Ge, Y. Ji, Z. Zhang, S. Zang, Y. Tian, H. Yu, M. Chen, G. Jiao, and D. Zhang, "Experiment study on the combustion performance of hydrogen-enriched natural gas in a DLE burner," Int. J. Hydrogen Energy, vol. 44, no. 26, pp. 14023-14031, 2019, doi: 10.1016/j.ijhydene.2019.03.257.

[6] P. Sun, Z. Zhang, Z. Li, Q. Guo, and F. Dong, "A Study of Two Dimensional Tomography Reconstruction of Temperature and Gas Concentration in a Combustion Field Using TDLAS," Applied Sciences, vol. 7, no. 10, p. 990, 2017, doi: 10.3390/app7100990.

[7] Z. Ahmadi and M. Zabetian Targhi, "Thermal performance investigation of a premixed surface flame burner used in the domestic heating boilers," Energy, vol. 236, 2021, doi: 10.1016/j.energy.2021.121481.

[8] J. Li, H. Huang, Y. Bai, S. Li, and N. Kobayashi, "Combustion and heat release characteristics of hydrogen/air diffusion flame on a micro-jet array burner," International Journal of Hydrogen Energy, vol. 43, no. 29, pp. 13563-13574, 2018, doi: 10.1016/j.ijhydene.2018.04.195.

[9] Q. Qi, M. M. Hossain, J. Li, B. Zhang, J. Li, and C. Xu, "Approach to reduce light field sampling redundancy for flame temperature reconstruction," Optics express, vol. 29, no. 9, pp. 13094-13114, 2021, doi: 10.1364/OE.424112.

[10] R. Ng, M. Levoy, M. Brédif, G. Duval, M. Horowitz, and P. Hanrahan, "Light field photography with a hand-held plenoptic camera," Stanford university, 2005.

[11] Zhao W , Zhang B , and X. C, "Optical Sectioning Tomographic Reconstruction of Three-dimensional Flame Temperature Distribution Using Single Light Field Camera," IEEE Sensors Journal, vol. 18, no. 3, pp. 528-539, 2018, doi: 10.1109/JSEN.2017.2772899.

[12] Y. Liu, M. Zhu, T. Wang, G. Lei, M. M. Hossain, B. Zhang, J. Li,and X. Chuan, "Spatial resolution of light field sectioning pyrometry for flame temperature measurement," Opt Laser Eng, vol. 140, pp. 106545, 2021, doi: https://doi.org/10.1016/j.optlaseng.2021.106545.

[13] J. Sun, C. Xu, B. Zhang, M. M. Hossain, S. Wang, H. Qi, and H. Tan, "Three-dimensional temperature field measurement of flame using a single light field camera," Optics express, vol. 24, no. 2, pp. 1118-1132, 2016, doi: 10.1364/OE.24.001118.

[14] D. G. Dansereau, O. Pizarro, and S. B. Williams, "Linear Volumetric Focus for Light Field Cameras," ACM Trans. Graph., vol. 34, no. 2, pp.1-20 , 2015, doi: 10.1145/2665074.

[15] K. Masaoka, T. Yamashita, Y. Nishida, and M. Sugawara, "Modified slanted-edge method and multidirectional modulation transfer function estimation," Opt. Express, vol. 22, no. 5, pp. 6040-6046, 2014, doi: 10.1364/OE.22.006040.